WIND-TUNNEL BUFFETING MEASUREMENTS ON TWO WING—END-PLATE AIRPLANE MODEL CONFIGURATIONS

by William B. Igoe

Langley Research Center
Langley Station, Hampton, Va.

WIND-TUNNEL BUFFETING MEASUREMENTS ON TWO WING — END-PLATE

AIRPLANE MODEL CONFIGURATIONS

By William B. Igoe

Langley Research Center
Langley Station, Hampton, Va.

NATIONAL AERONAUTICS AND SPACE ADMINISTRATION

WIND-TUNNEL BUFFETING MEASUREMENTS ON TWO WING—END-PLATE
AIRPLANE MODEL CONFIGURATIONS

By William B. Igoe
Langley Research Center

SUMMARY

During the course of wind-tunnel force tests on a 1/30-scale model of a proposed subsonic nuclear-powered airplane in the Langley 16-foot transonic tunnel, wing-buffeting measurements were made on two different wing—end-plate model configurations. The low-aspect-ratio (3.6) wing had a leading-edge sweepback angle of 51°, and the high-aspect-ratio (6.0) wing had a leading-edge sweepback angle of 36°. The model support system introduced undesirable buffeting response vibration modes in the same frequency range as the model wing vibration modes. On a comparative basis, the high-aspect-ratio wing configuration generally exhibited a more abrupt entry into buffeting with increasing angle of attack and had a lower lift coefficient for the onset of buffeting than that of the low-aspect-ratio wing configuration.

INTRODUCTION

The buffeting measurements presented in this report were obtained during the course of conventional wind-tunnel force tests which were reported in references 1 and 2. Time-history records of the wing bending moments on an airplane model were obtained to compare the buffeting characteristics of two different wing configurations and to predict full-scale-airplane flight wing-buffeting characteristics from the wind-tunnel model measurements.

Some of the wind-tunnel testing techniques for making these measurements have been discussed in references 3 and 4. Reference 4 has indicated that the principal model requirements for flight buffeting prediction are (1) that the model wing damping be primarily aerodynamic so that differences between model and full-scale structural damping will be unimportant and (2) that the model buffeting response mode and scaled reduced frequency correspond to those of the airplane. Flight buffeting measurements (ref. 3) have shown that the airplane wing buffeting response usually occurs primarily in the wing first mode of vibration. During the wind-tunnel tests of references 1 and 2, the model support system introduced buffeting response modes in the same frequency range as the model wing vibration modes. These extraneous response modes would not be duplicated

in the full-scale-airplane flight buffeting response.   Because of their presence, no attempt has been made to predict full-scale buffeting loads from the model data.   However, since the support system was the same for the two model wing configurations, their buffeting characteristics may be compared on a relative basis, and buffet boundaries defined where possible.

The buffeting measurements were made in the Langley 16-foot transonic tunnel on a 1/30-scale model of a proposed subsonic nuclear-powered airplane.   One wing configuration (reported in ref. 1) had an aspect ratio of 3.6 and a leading-edge sweepback angle of 51°; the other (reported in ref. 2) had an aspect ratio of 6.0 and a leading-edge sweepback angle of 36°.   Both wings had end plates which acted as wing-tip-mounted vertical fins.

SYMBOLS

b   wing span, meters (m)

$c(y)$ wing chord, meters (m)

c_{av} average wing chord, meters (m)

C_B aerodynamic coefficient of buffeting intensity (called buffeting coefficient herein), $\dfrac{\sigma}{\omega_1 M_{m,1} S_1 \left(\dfrac{\pi c_{av}}{2 M_1 S_2}\right)^{1/2} q^{1/2}}$

C_L lift coefficient, $\dfrac{\text{Lift}}{qS}$

f   frequency, cps

$m(y)$ mass per unit length of wing, kilograms/meter (kg/m)

M   Mach number

M_1 weighted wing mass, $\displaystyle\int_{-b/2}^{b/2} m(y)\left[w_1(y)\right]^2 dy$, kilograms (kg)

$M_{m,1}$ weighted wing moment of mass outboard of point y_g,

$$\int_{y_g}^{b/2} (y - y_g)m(y)w_1(y)dy, \text{ kilogram-meters (kg-m)}$$

q dynamic pressure, newtons/meter^2 (N/m^2)

S planform area of basic wing (excludes leading-edge chord-extension), meters2 (m^2)

S_1 weighted wing area, $\int_{-b/2}^{b/2} c(y)w_1(y)dy$, meters^2 (m^2)

S_2 weighted wing area, $\int_{-b/2}^{b/2} c(y)\left[w_1(y)\right]^2 dy$, meters^2 (m^2)

$w_1(y)$ deflection of wing elastic axis in first symmetrical mode of vibration, normalized to unit deflection at wing tip

y spanwise coordinate, meters (m)

y_g spanwise coordinate at strain-gage location, meters (m)

α angle of attack of wing chord plane, degrees (deg)

$\Delta\alpha$ root-mean-square turbulent-fluctuating-airstream angularity on wind-tunnel center line in pitch plane of model, radians (rad)

σ root-mean-square wing bending moment measured at strain-gage location, newton-meters (N-m)

ω_1 wind-off natural circular frequency of wing first symmetrical mode, radians/second (rad/sec)

APPARATUS AND TESTS

Model

A photograph of the 1/30-scale model with the low-aspect-ratio (3.6) wing is presented in figure 1, and sketches of both models together with a few of the overall dimensions are presented in figure 2. Some of the model geometrical and physical constants

are presented in table I. The model consisted of a wing with end plates, a fuselage, and flow-through nacelles. A complete description of all the model components is presented in references 1 and 2. The low-aspect-ratio (3.6) wing had a leading-edge sweepback angle of 51°, a root-chord incidence angle of 1.5^O, and an outboard leading-edge chord-extension deflected down 15°. The high-aspect-ratio (6.0) wing had a leading-edge sweepback angle of 36°, a root-chord incidence angle of 3.5^O, and an outboard leading-edge chord-extension deflected down 12°. Each wing was built up of solid steel components. Both wings had a basic planform taper ratio of 0.4 and a dihedral angle of 4°. Each wing had modified NACA 65-series airfoil sections streamwise, with slightly different thickness-chord ratio distributions which varied from about 0.12 at the root to about 0.08 at the tip. The fuselage, nacelles, and entire model support system were the same for both configurations. Neither wing was twisted or cambered.

The wind-on model frequency characteristics are shown in the power spectral density plots of the wing bending moment in figures 3 and 4. The important response modes are the wing first symmetric and second antisymmetric modes, and the "rigid body" roll and pitch modes which are introduced by the support system.

Instrumentation

The wing-buffeting data were obtained by using a bending strain-gage bridge which was mounted near the elastic axis on the left-wing panel of each configuration, about one-quarter of a meter outboard of the model center line. The strain-gage locations are shown in figure 2. The time-history strain-gage signals were amplified and recorded on a 14-channel magnetic-tape recorder utilizing a frequency modulation system. In order to obtain root-mean-square and power-spectral-density information, the tape records were analyzed on analog data-reduction equipment which is described in reference 5.

As a measure of wind-tunnel turbulence, the time-history of the fluctuating differential between static-pressure orifices on the top and bottom of a 3° cone was obtained with a miniature electrical pressure gage of the type described in reference 6. The gage was installed inside the cone between the differential static-pressure orifices. Reference 6 shows the frequency response of this type of pressure-gage installation to be flat to more than 500 cps. The fluctuating differential pressure signal was tape recorded and analyzed for the root-mean-square and power-spectral-density information. A steady-state calibration of the cone static-pressure differential with cone angle of attack was obtained as a function of Mach number. The analyses of the fluctuating cone static-pressure differential were then interpreted as a measure of the wind-tunnel airstream turbulence on the tunnel center line in the pitch plane of the model using the steady-state calibration.

The model steady-state aerodynamic forces were obtained with a six-component internal strain-gage balance, and the model steady-state angle of attack was determined with an internal pendulum-type attitude indicator.

Wind Tunnel

The model was tested in the Langley 16-foot transonic tunnel, which is a single-return wind tunnel with a slotted octagonal test section operating at atmospheric stagnation pressure. (See ref. 7.) The model support system utilized a sting mount from the rear (fig. 1) and pivoted so that the model remained near the center of the test section throughout the angle-of-attack range.

The power spectral density of the airstream turbulence, as inferred from the 3° cone fluctuating differential static-pressure measurements, is shown in figure 5 for a representative Mach number of 0.80. A large portion of the power is concentrated at frequencies below 10 cps. The variation with Mach number of the root-mean-square turbulent-fluctuating-airstream angularity from the 3° cone measurements is shown in figure 6.

Tests

The low-aspect-ratio wing configuration was tested at Mach numbers from 0.30 to 0.98 and at angles of attack from -1.5^O to 16.5^O; the high-aspect-ratio wing configuration was tested at Mach numbers from 0.60 to 0.92 and at angles of attack from -1.5^O to 18.5^O. The test Reynolds number per meter varied approximately from 6×10^6 to 13×10^6. Boundary-layer transition was fixed during the buffeting tests with distributed-roughness-particle transition strips located near the nose or leading edge of all model components. The transition strips consisted of No. 120 grit size silicon carbide grains sparsely distributed in a thin film of shellac. The streamwise dimensions and locations of the transition strips were approximately as follows: On the wing, a 1.0-centimeter-wide strip was parallel to and 1.5 centimeters behind the leading edge; on the end plates and nacelles, a 0.6-centimeter-wide strip was parallel to and 1.0 centimeter behind the leading edge; and on the fuselage, a 0.6-centimeter-wide circumferential strip was 1.9 centimeters behind the nose. The longitudinal trim control surfaces (free-floating canards located near the nose of the fuselage) were not present for either configuration during the buffeting tests.

The steady-state and time-history data were recorded concurrently during the buffeting tests. A tape record of about 45 seconds duration was obtained of the wing strain-gage output at each data point for subsequent analysis. The model wind-off frequency response characteristics were determined in the tunnel and on a ground stand by shaking the model with an electromagnetic shaker.

RESULTS AND DISCUSSION

The buffeting results are presented in figure 7 for the low-aspect-ratio (3.6) wing configuration and in figure 8 for the high-aspect-ratio (6.0) wing configuration. These figures show the buffeting coefficient C_B as a function of wing angle of attack at various Mach numbers. The steady-state lift coefficient C_L is included in the figures for reference purposes.

At low angles of attack for most Mach numbers, the response is similar for both wing configurations but the high-aspect-ratio wing configuration appears more susceptible to the exciting forces which are present under low lift conditions. These exciting forces are considered to be caused primarily by wind-tunnel airstream turbulence. During buffeting tests, such forces are undesirable because their presence may tend to change or obscure the buffeting response. The method of subtracting the effects of turbulence from buffeting loads data depends on the correlation which exists between the loads due to turbulence and those due to buffeting, and must be regarded as somewhat uncertain because of the limited amount of information which is available on this subject. Because of this uncertainty, the effects of turbulence have not been subtracted from the buffeting data of figures 7 and 8.

As may be seen in figure 7, the low-aspect-ratio (3.6) wing exhibited a gradual entry into buffeting with increasing angle of attack at Mach numbers up to 0.80. Severe nonlinearities in the lift curve occurred at a Mach number of 0.90 and at an angle of attack of about 8.5°. (See fig. 7(e).) The data points of the buffeting tests were not spaced closely enough to define the nonlinearities but subsequent force tests revealed these nonlinearities. (See fig. 20 of ref. **1.)** These nonlinearities were accompanied by an abrupt increase in the buffeting coefficient at this Mach number. Figure 8 shows that at all Mach numbers from 0.60 to 0.92, the high-aspect-ratio (6.0) wing configuration exhibited a more abrupt entry into buffeting with increasing angle of attack than the low-aspect-ratio wing. If the lift coefficient for the onset of buffeting is arbitrarily taken as occurring at the angle of attack where the dashed lines intersect in figures 7 and 8, then the resulting buffet boundaries are as shown in figure 9. The lift coefficient for the onset of buffeting on the high-aspect-ratio (6.0) wing is seen to be lower than that for the low-aspect-ratio (3.6) wing.

CONCLUDING REMARKS

During the course of wind-tunnel force tests on a 1/30-scale model of a proposed subsonic nuclear-powered airplane in the Langley 16-foot transonic tunnel, wing-buffeting measurements were made on two different wing —end-plate model configurations. The low-aspect-ratio (3.6) wing had a leading-edge sweepback angle of 51°, and the

high-aspect-ratio (6.0) wing had a leading-edge sweepback angle of 36°. The model support system introduced undesirable buffeting response vibration modes in the same frequency range as the model wing vibration modes. On a comparative basis, the high-aspect-ratio wing configuration generally exhibited a more abrupt entry into buffeting with increasing angle of attack and had a lower lift coefficient for the onset of buffeting than that of the low-aspect-ratio wing configuration.

Langley Research Center,
    National Aeronautics and Space Administration,
        Langley Station, Hampton, Va., March 30, 1967,
            126-13-01-03-23.

REFERENCES

1. Igoe, William B.; Re, Richard J.; and Capone, Francis J.:   Longitudinal Aerodynamic Characteristics of a 1/30-Scale Subsonic Canard-Airplane Model Having a Wing With an Aspect Ratio of 3.6 at Mach Numbers From 0.30 to 0.98.   NASA TM X-669, 1962.

2. Igoe, William B.; Capone, Francis J.; and Re, Richard J.:   Subsonic Longitudinal Aerodynamic Characteristics of a 1/30-Scale Canard-Airplane Model Having a Wing With an Aspect Ratio of 6.0.   NASA TM X-668, 1962.

3. Huston, Wilber B.; Rainey, A. Gerald; and Baker, Thomas F.:   A Study of the Correlation Between Flight and Wind-Tunnel Buffeting Loads.   NACA RM L55E16b, 1955.

4. Davis, Don D., Jr.; and Huston, Wilber B.:   The Use of Wind Tunnels to Predict Flight Buffet Loads.   NACA RM L57D25, 1957.

5. Smith, Francis B.:   Analog Equipment for Processing Randomly Fluctuating Data. Aeron. Eng. Rev., vol. 14, no. 5, May 1955, pp. 113-119.

6. Patterson, John L.:   A Miniature Electrical Pressure Gage Utilizing a Stretched Flat Diaphragm.   NACA TN 2659, 1952.

7. Ward, Vernon G.; Whitcomb, Charles F.; and Pearson, Merwin D.:   Air-Flow and Power Characteristics of the Langley 16-Foot Transonic Tunnel With Slotted Test Section.   NACA RM L52E01, 1952.

TABLE I. - MODEL GEOMETRICAL AND PHYSICAL CONSTANTS

	Low-aspect-ratio (3.6) wing	High-aspect-ratio (6.0) wing
$b/2$, m	0.682	0.880
c_{av}, m	0.379	0.293
y_g, m	0.268	0.253
S, m^2	0.490	0.488
S_1, m^2	0.085	0.095
S_2, m^2	0.048	0.052
M_1, kg	11.72	10.95
$M_{m,1}$, kg-m	2.67	3.86
ω_1, rad/sec	213	146
$\omega_1 M_{m,1} S_1 \left(\dfrac{\pi c_{av}}{2 M_1 S_2} \right)^{1/2}$, $\left[\left(\dfrac{\text{kg-m}}{\text{sec}^2} \right)^{1/2} \right] m2$	49.7	48.1
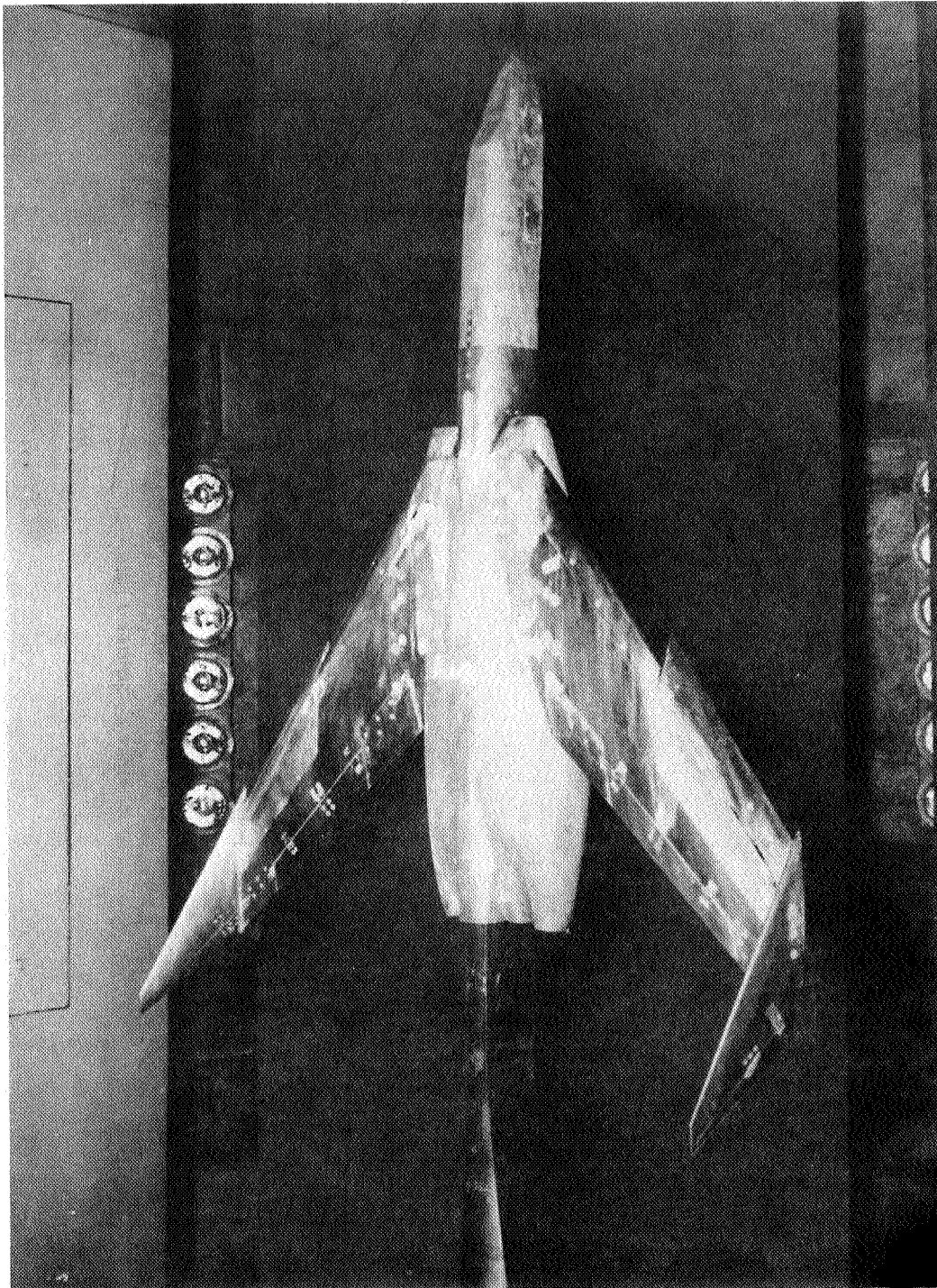
Figure 1.- Photograph of model of ratio (3.6) wing configuration in Langley 16-foot transonic tunnel.

L-60-1646.1

.268 m

50-percent-chord line

Strain gage

51°

.682 m
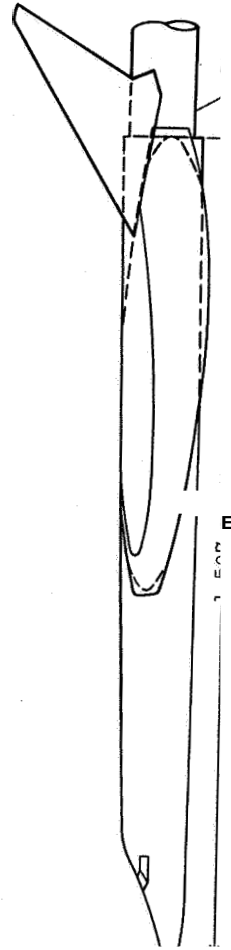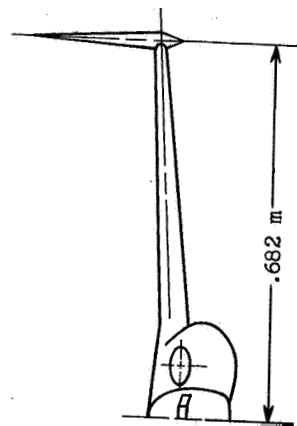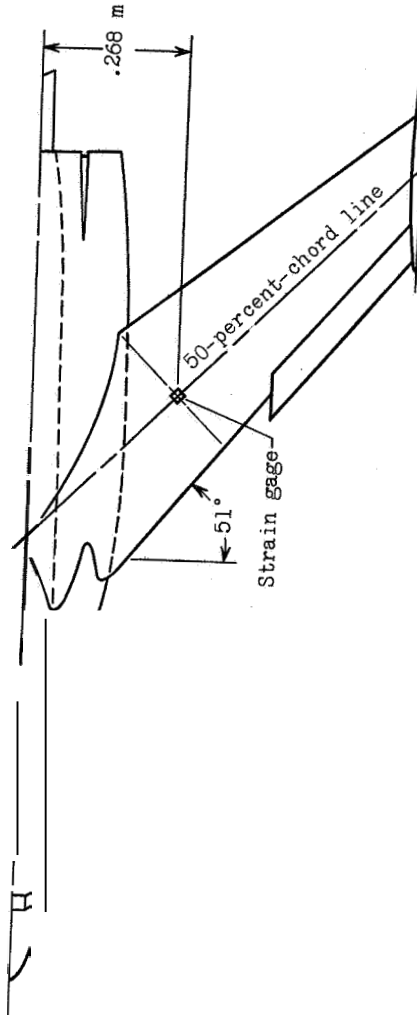
(a) Low-aspect-ratio (3.6) wing configuration.

Figure 2.- Sketches of model.

.253

50-percent-chord line

Strain gage

36°

E

Sting

1.507 m

.880 m
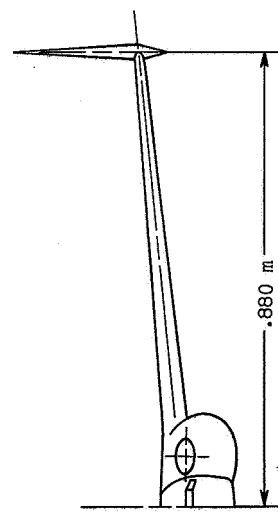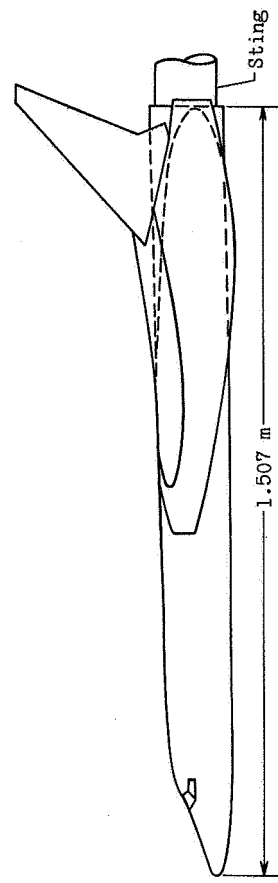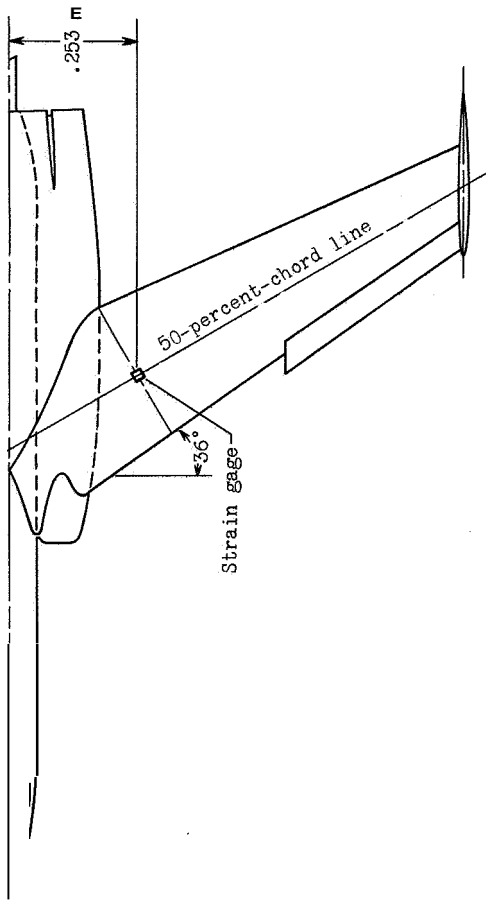
(b) High-aspect-ratio (6.0) wing configuration.

Figure 2.- Concluded.

11
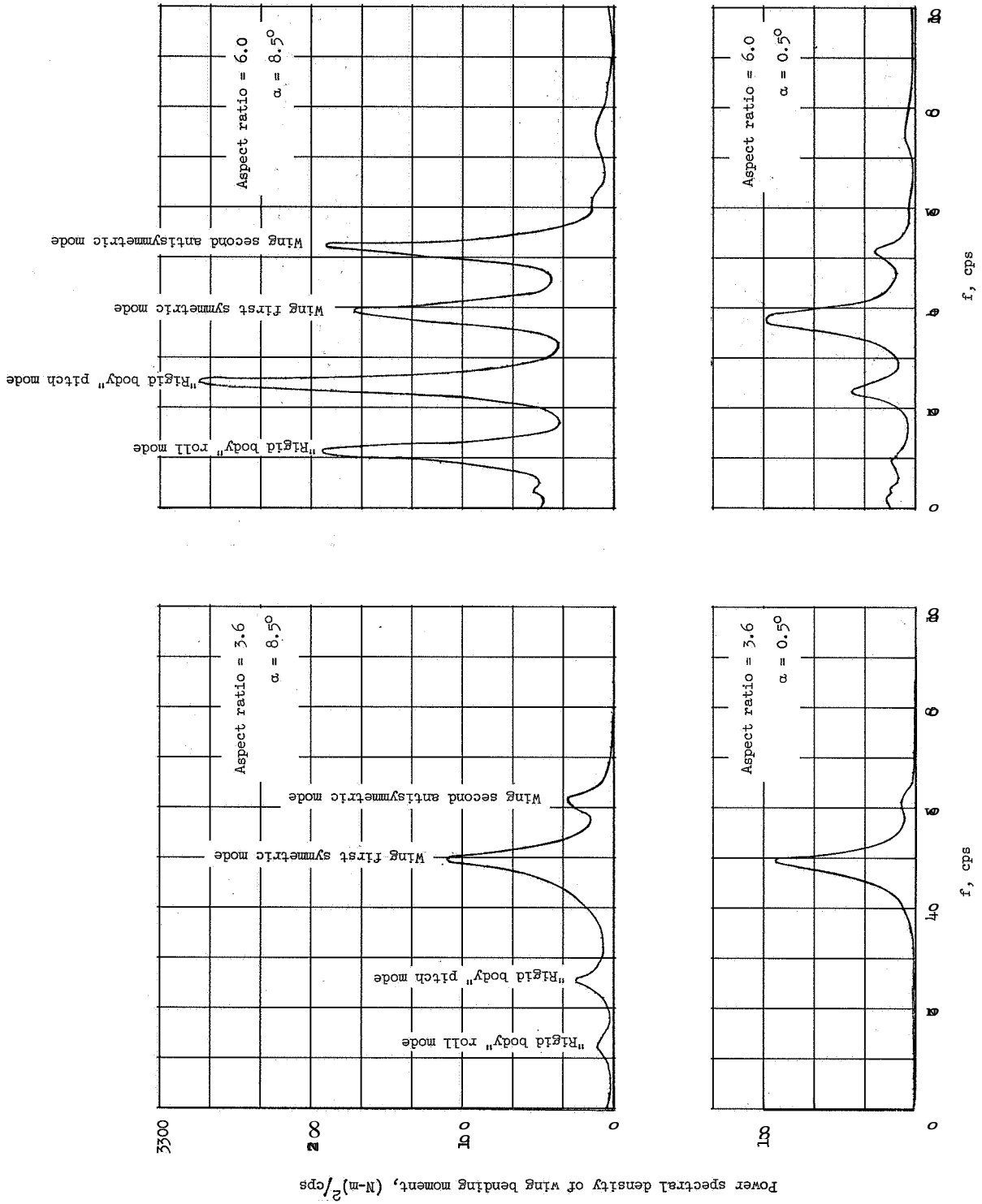
Figure 3.- Power spectral density of wing bending moment at M = 0.80.
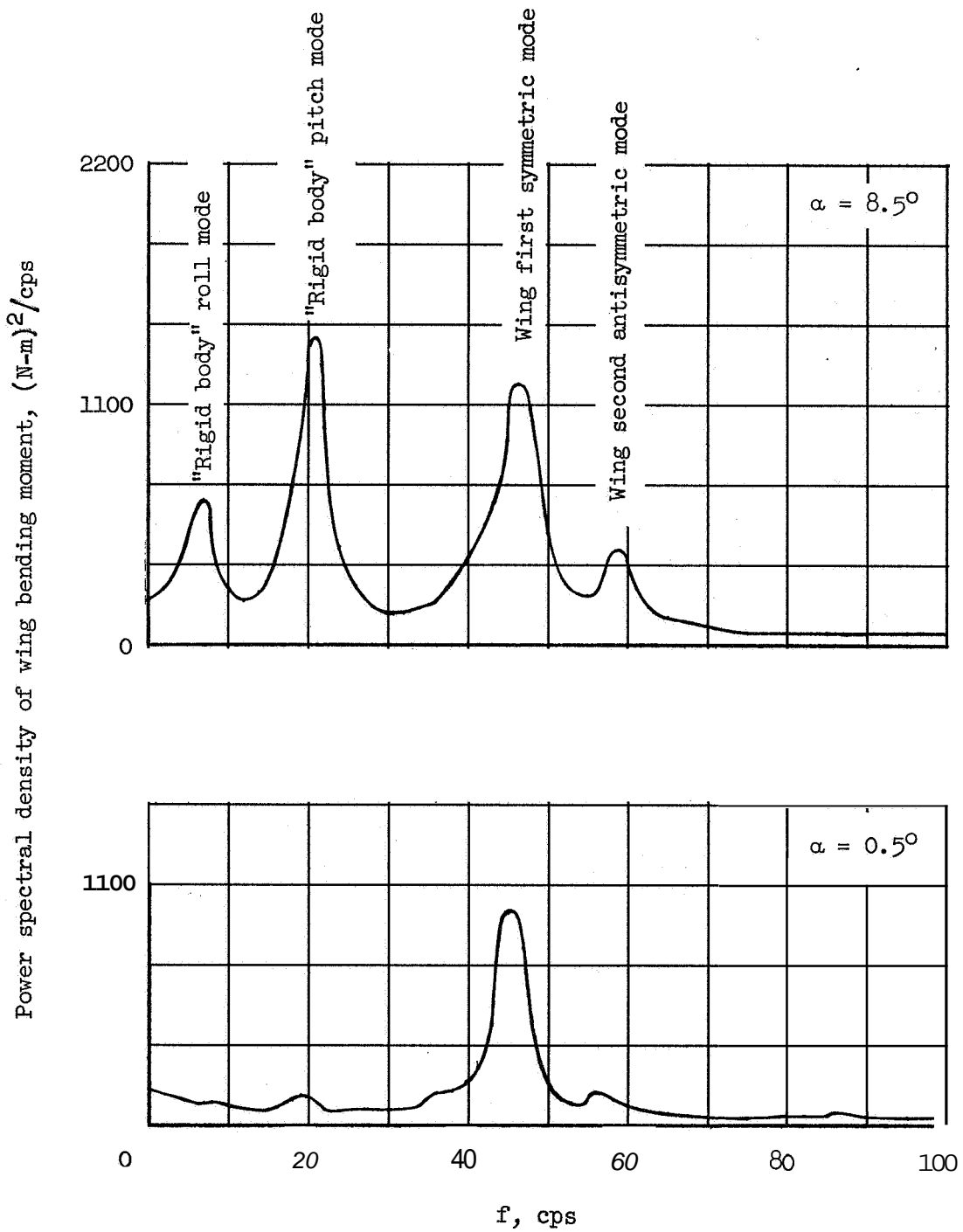
Figure 4.- Power spectral density of wing bending moment for low-aspect-ratio (3.6) wing at M = *0.90.*
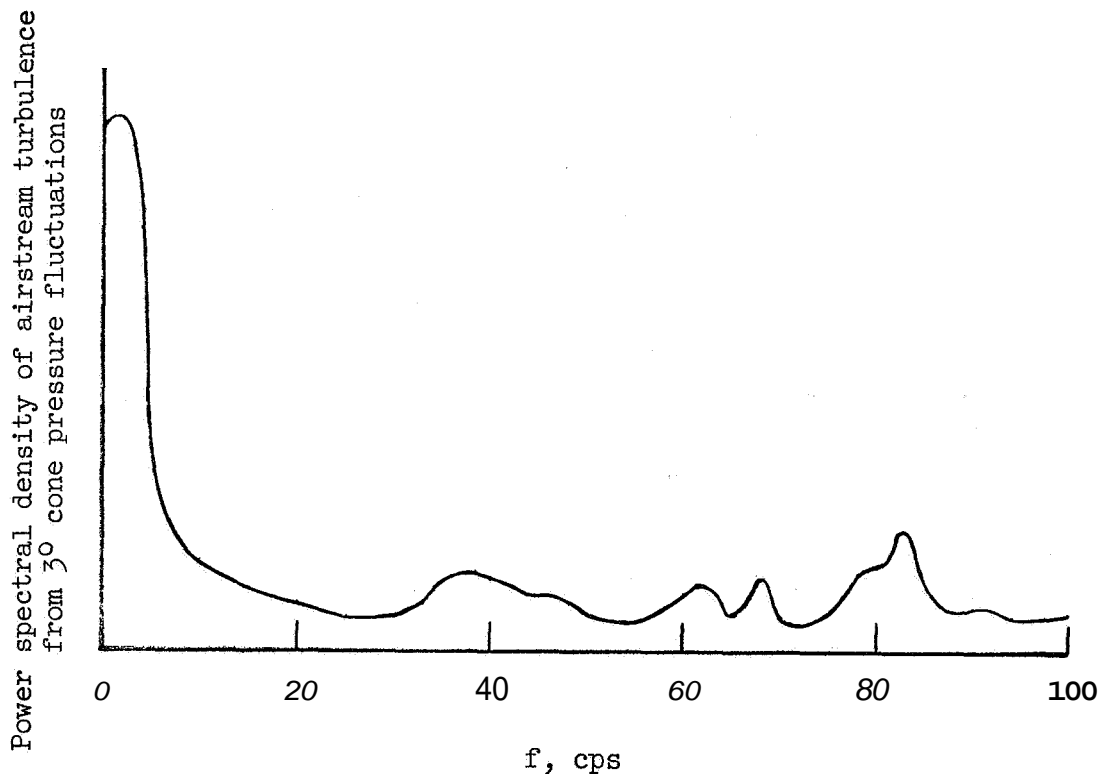
Figure 5.- Power spectral density of airstream turbulence from 3^0 cone pressure fluctuations at M = 0.80.
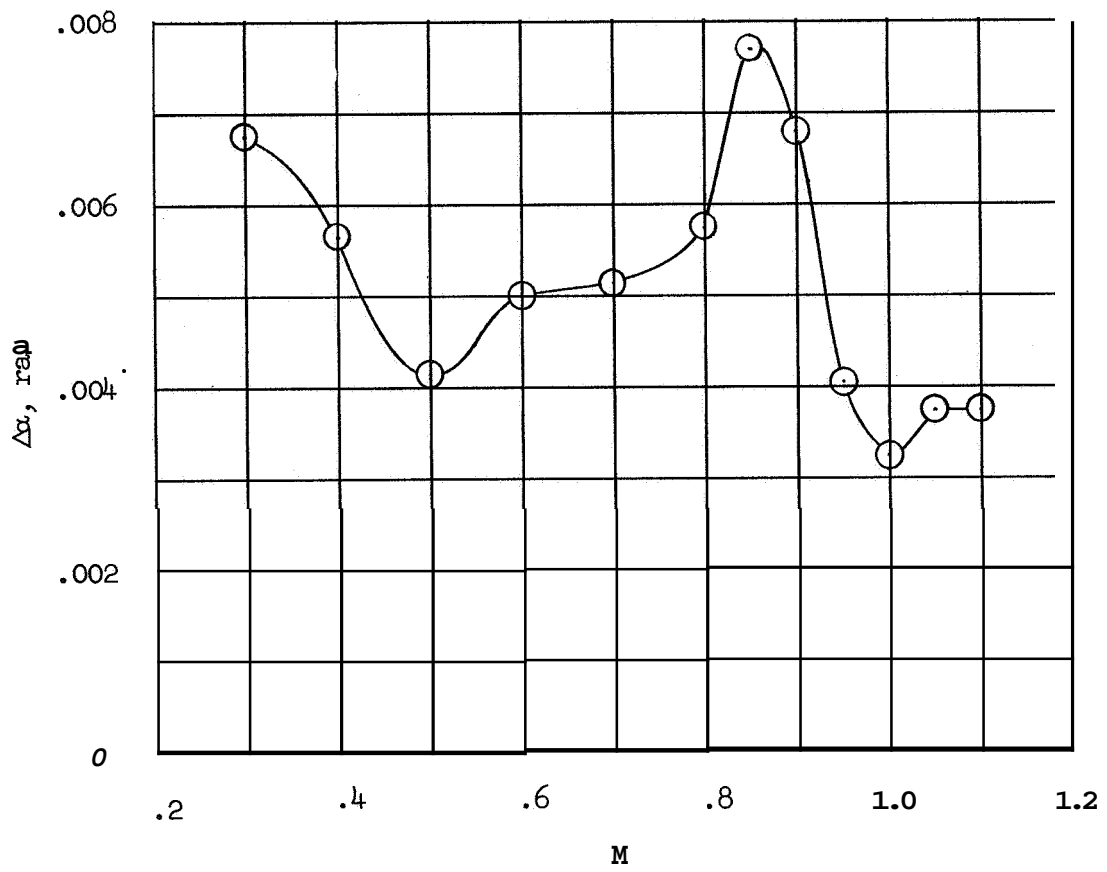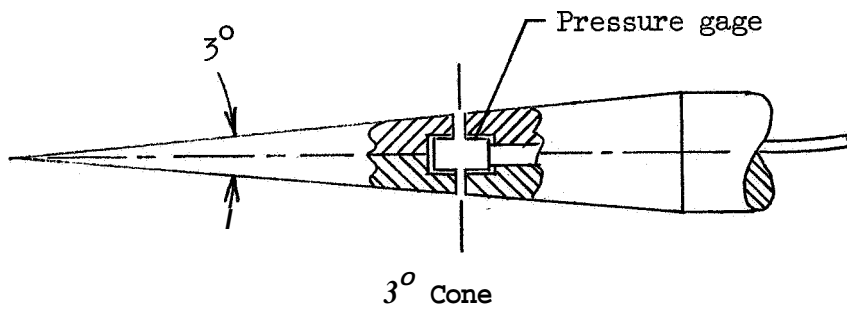
Figure 6- Variation with Mach number of turbulent-fluctuating-airstream angularity on wind-tunnel center line in pitch plane of model. (From 3⁰ cone data.)
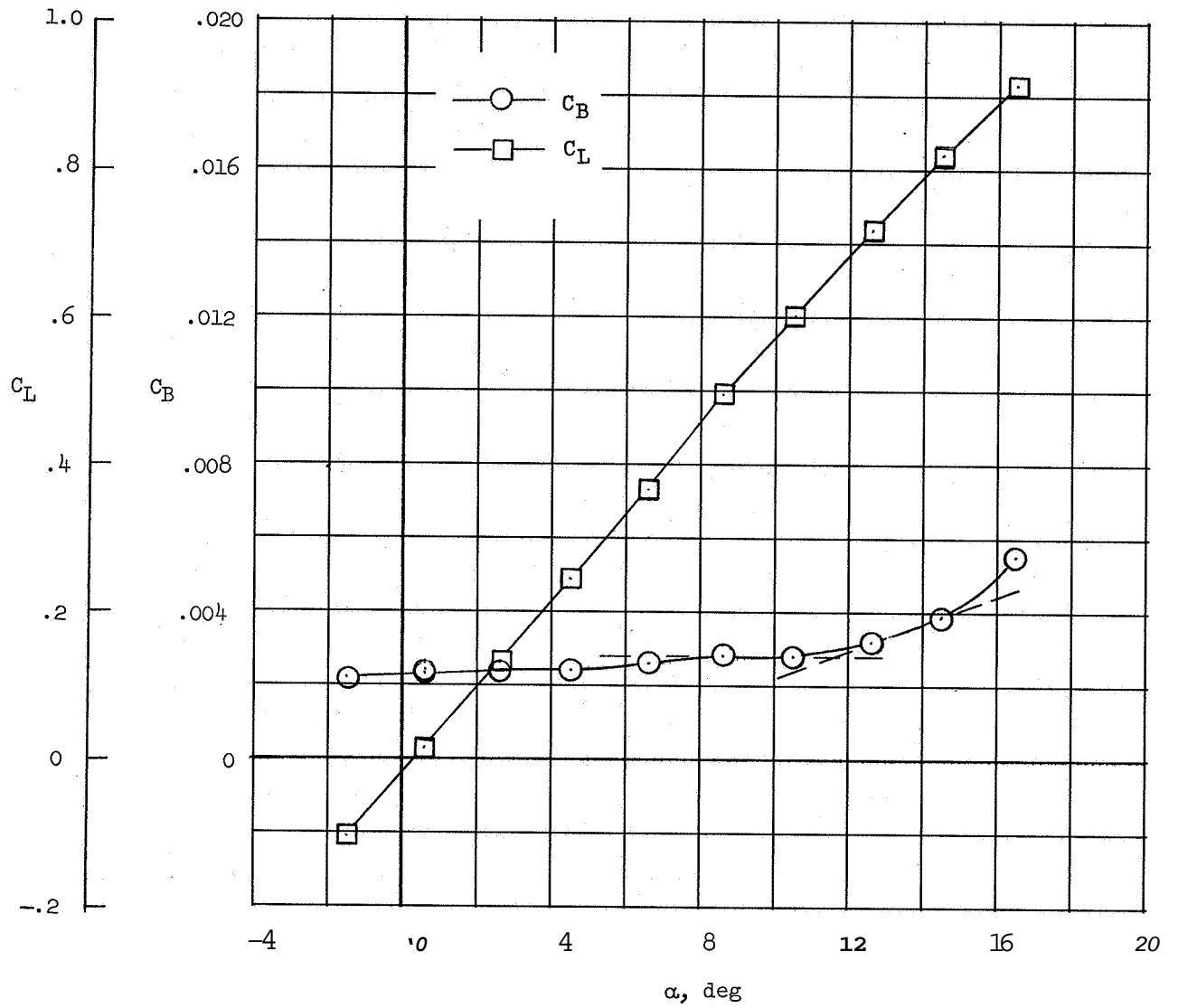
(a) M = 0.30.

Figure 7.- Variation of buffeting coefficient and lift coefficient with angle of attack for low-aspect-ratio 13.6) wing configuration. intersection of dashed lines indicates onset of buffeting.
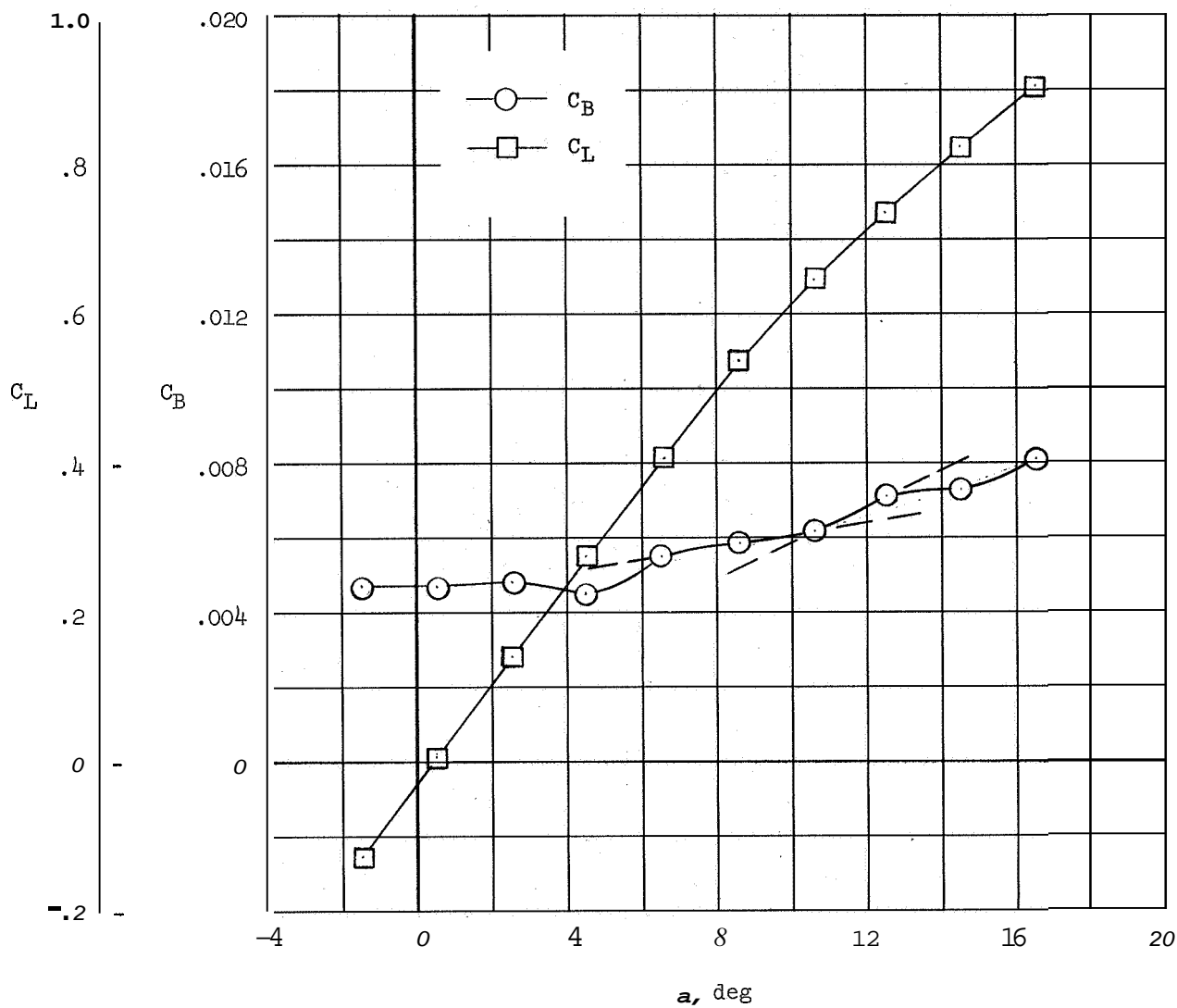
(b) M = 0.60.

Figure 7.- Continued.
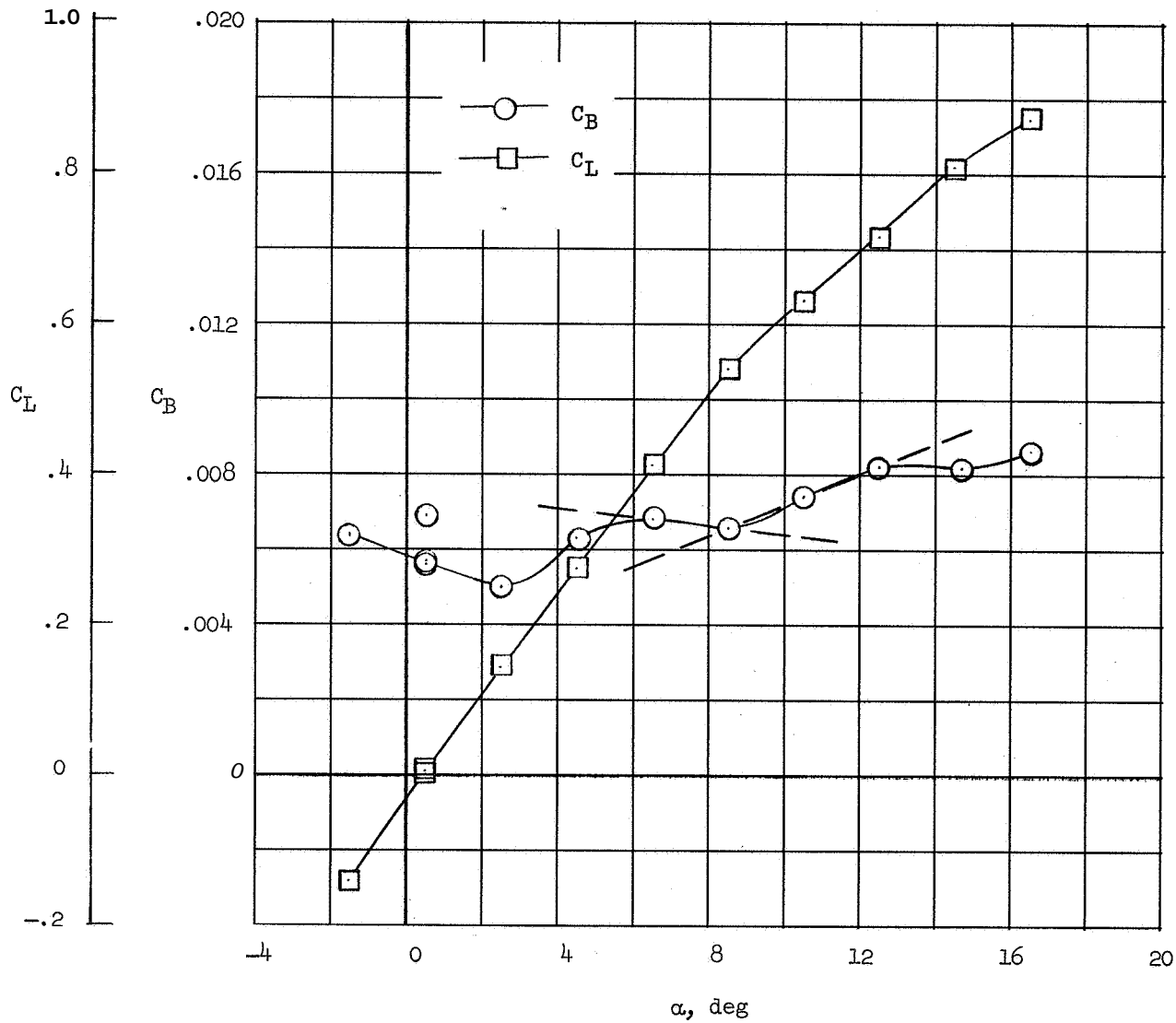
(c) M = 0.70.

Figure 7.- Continued.
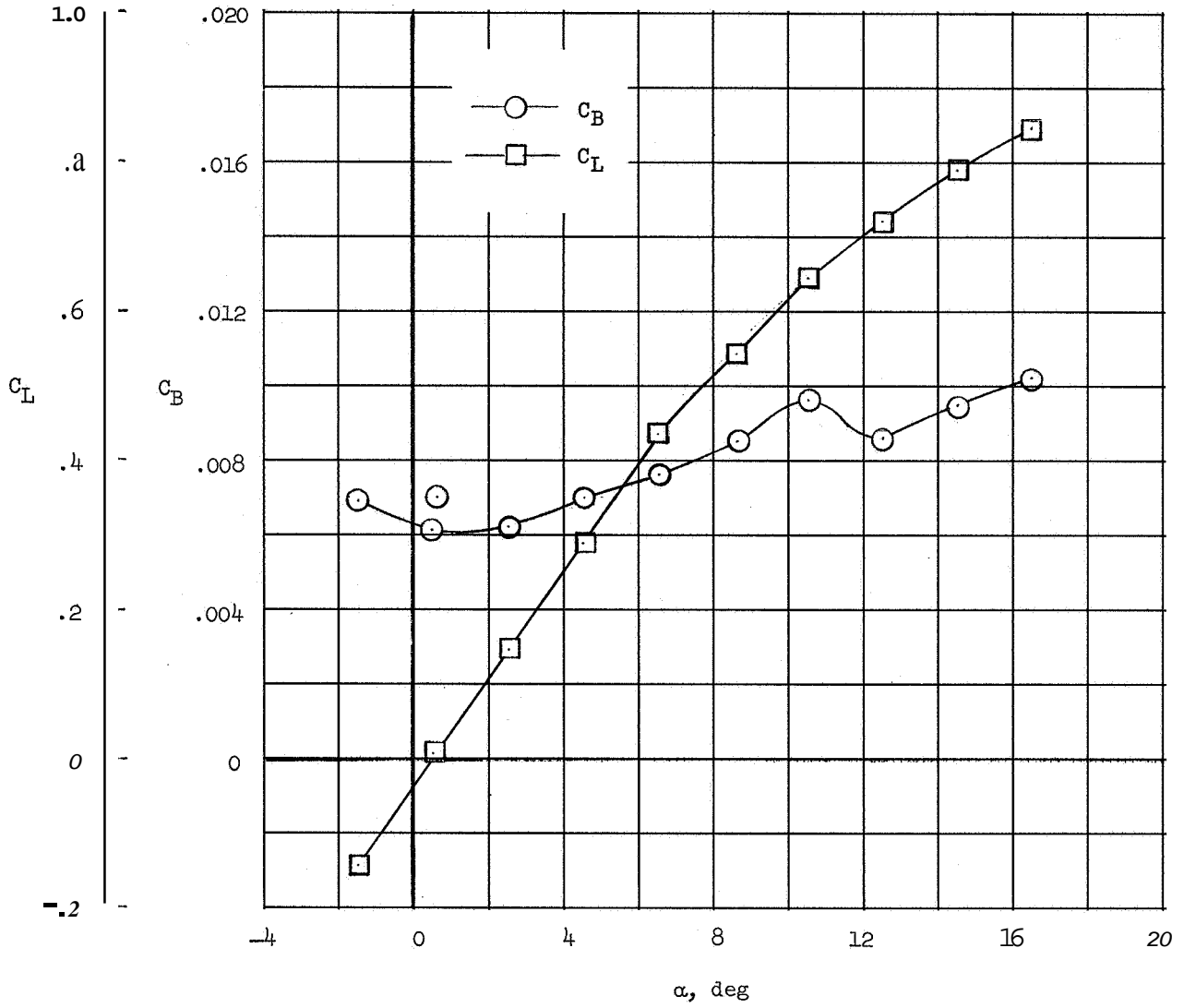
(d) M = 0.80.

Figure 7.- Continued.
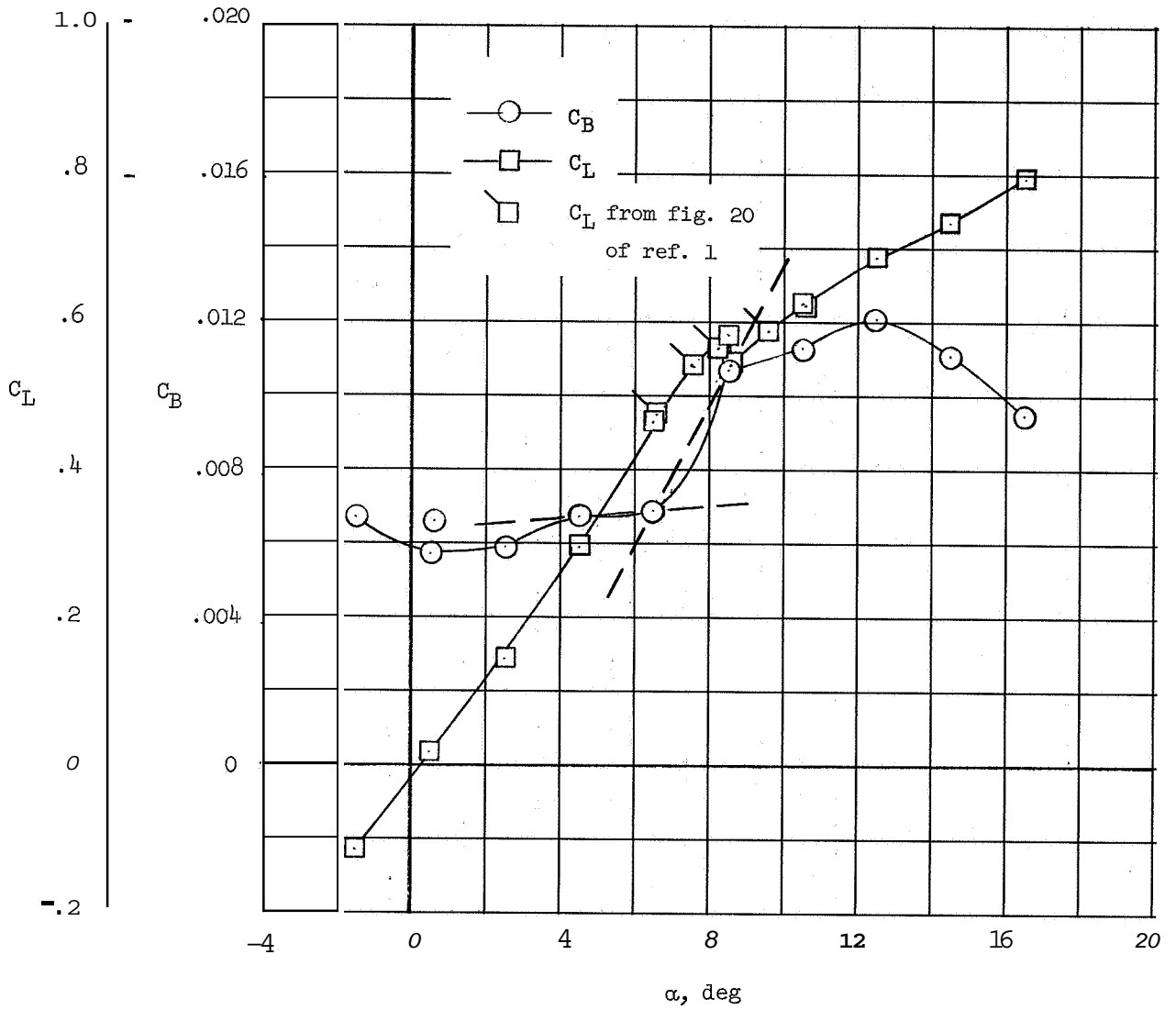
(e) M = 0.90.

Figure 7.- Continued.
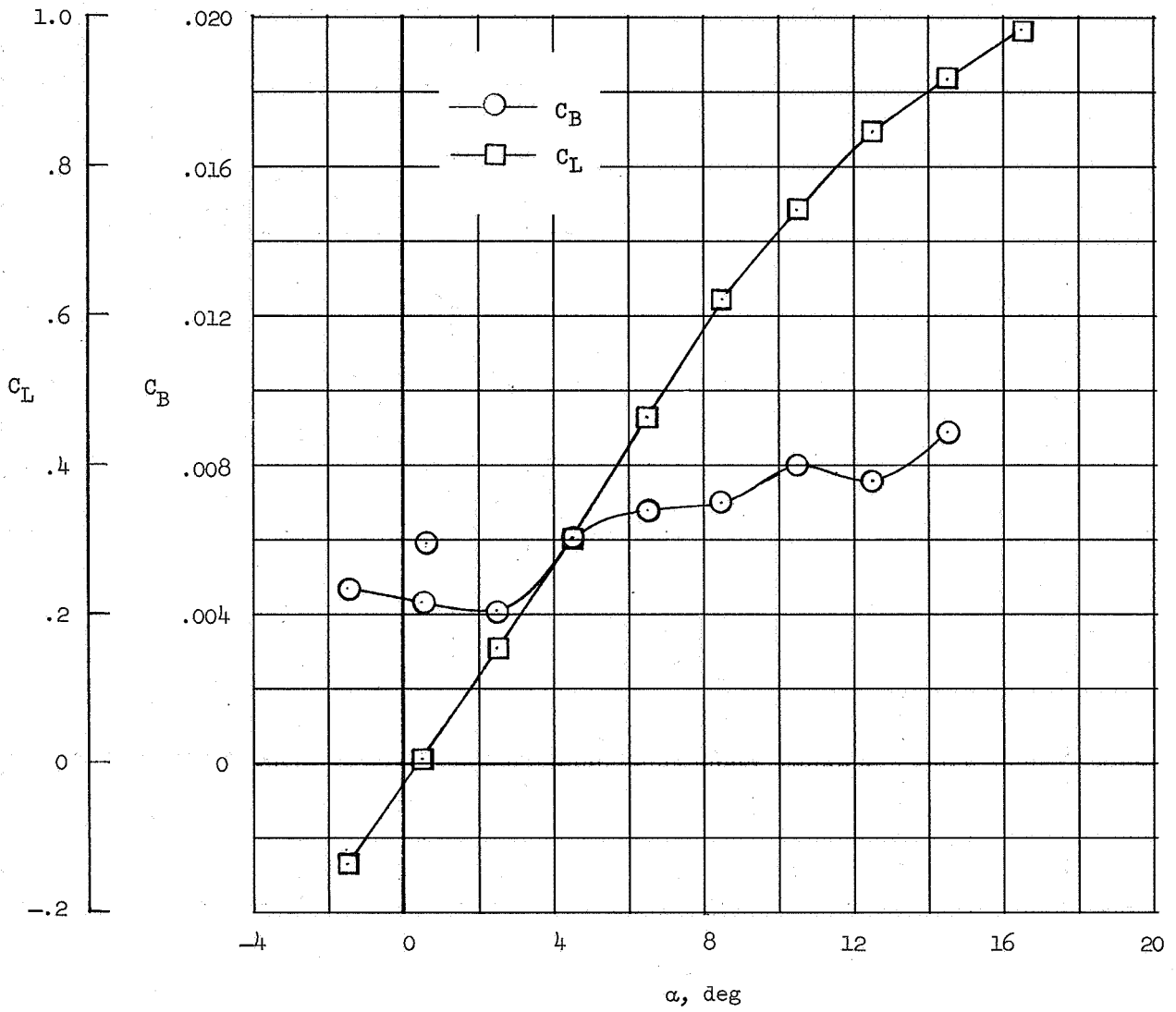
(f) M = 0.98.

Figure 7.- Concluded.
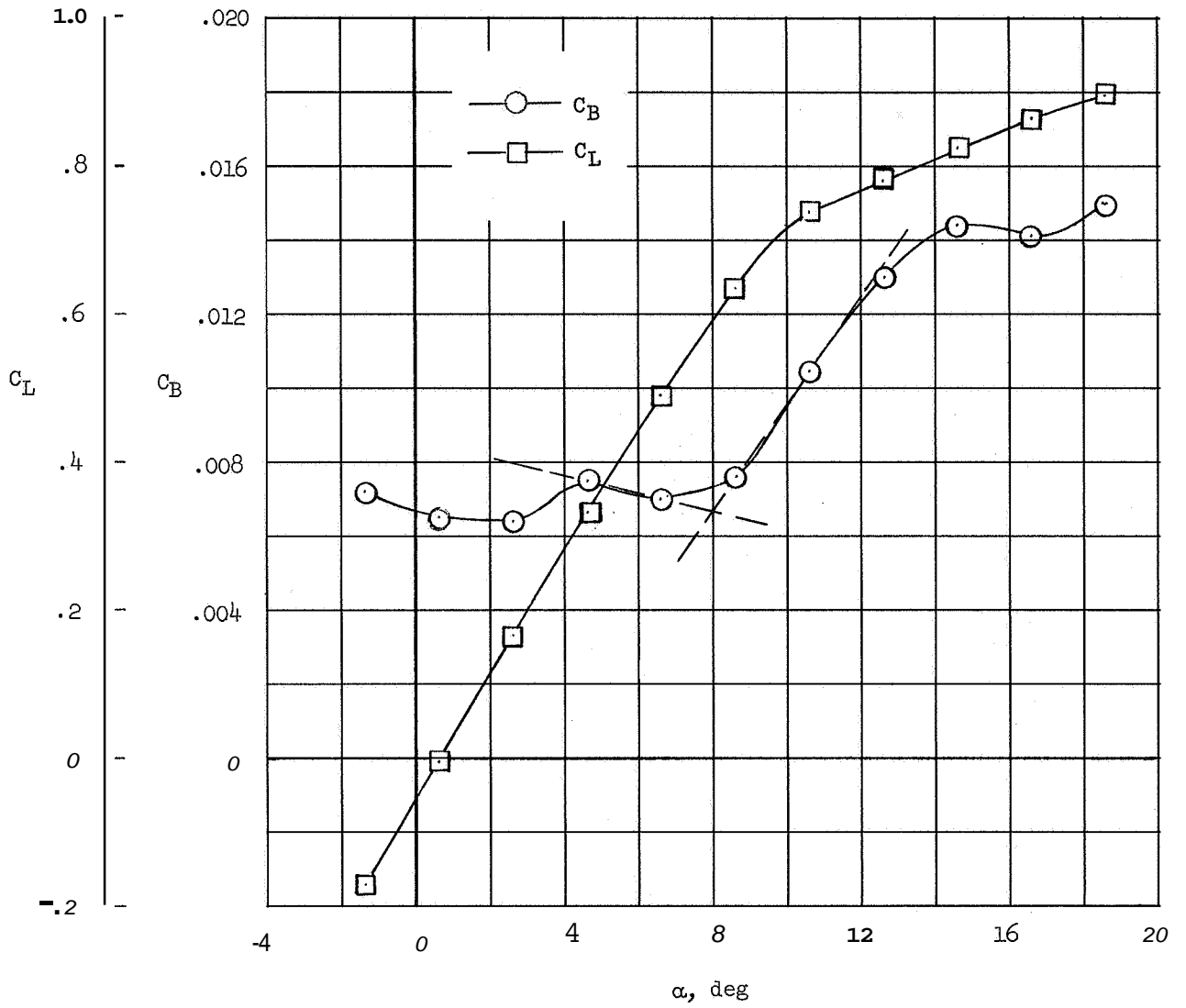
(a) M = 0.60.

Figure 8.- Variation of buffeting coefficient and lift coefficient with angle of attack for high-aspect-ratio (6.0) wing configuration. Intersection of dashed lines indicates onset of buffeting.
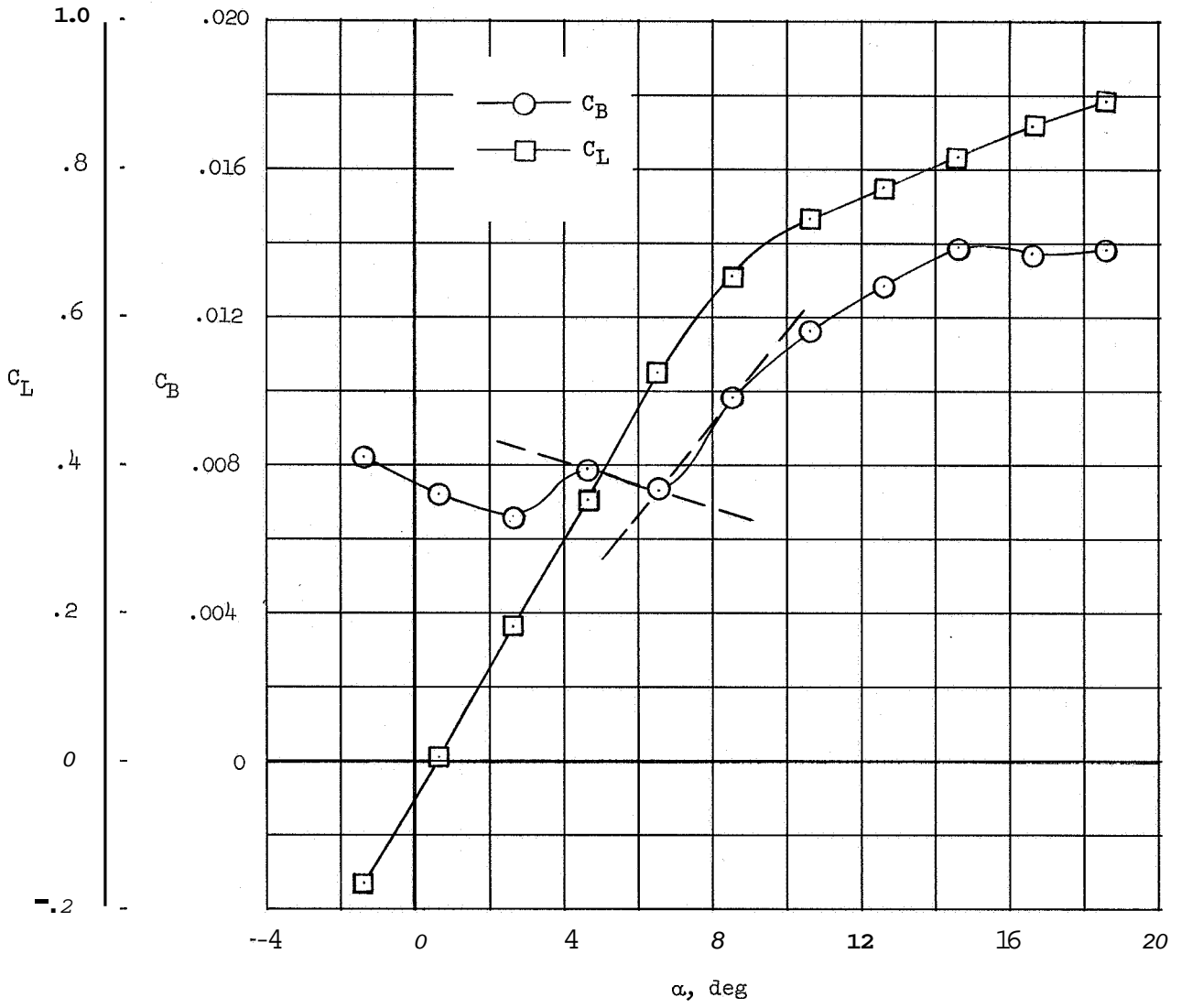
(b) M = 0.70.

Figure 8.- Continued.
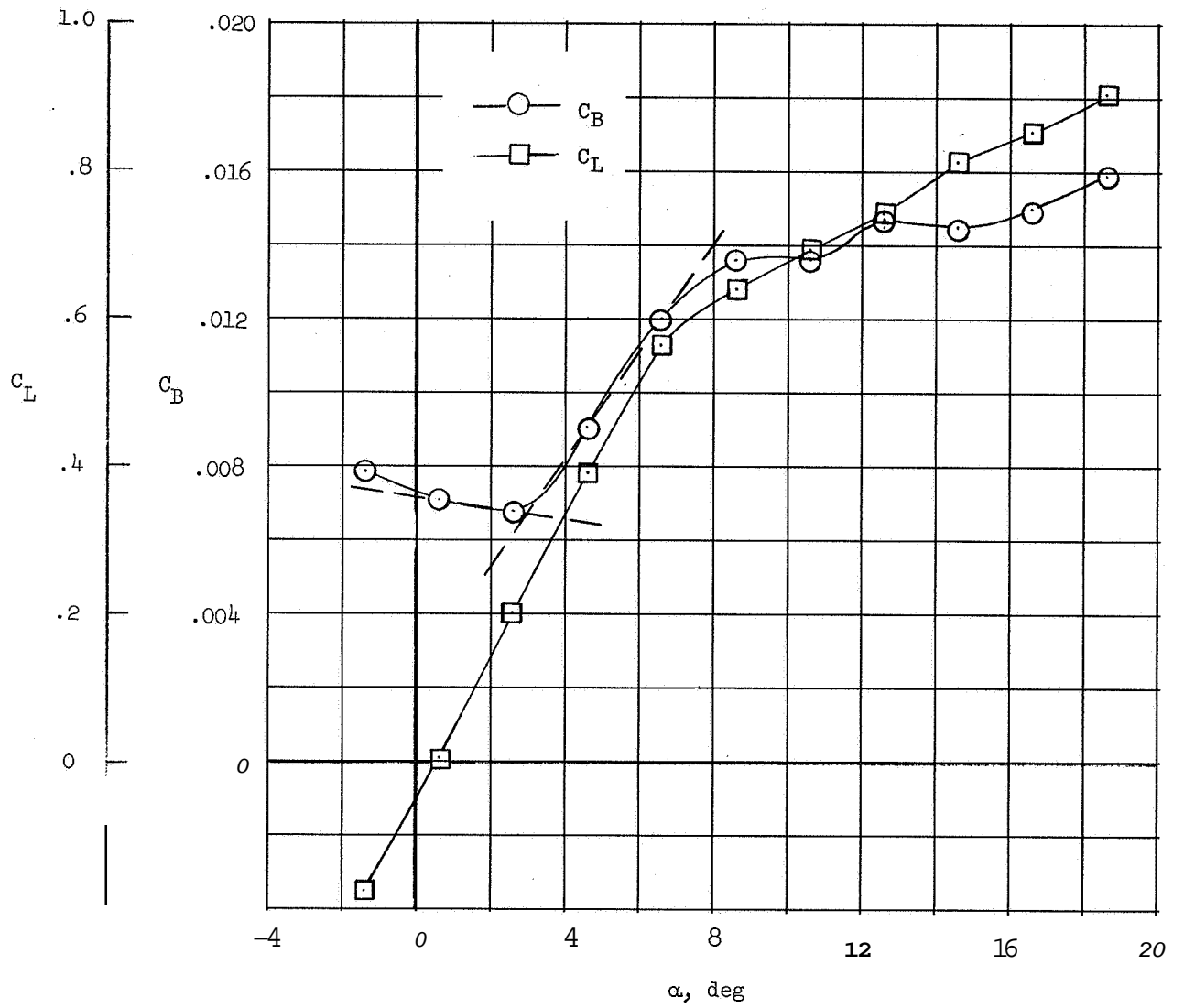
(c) M = 0.80.

Figure 8.- Continued.
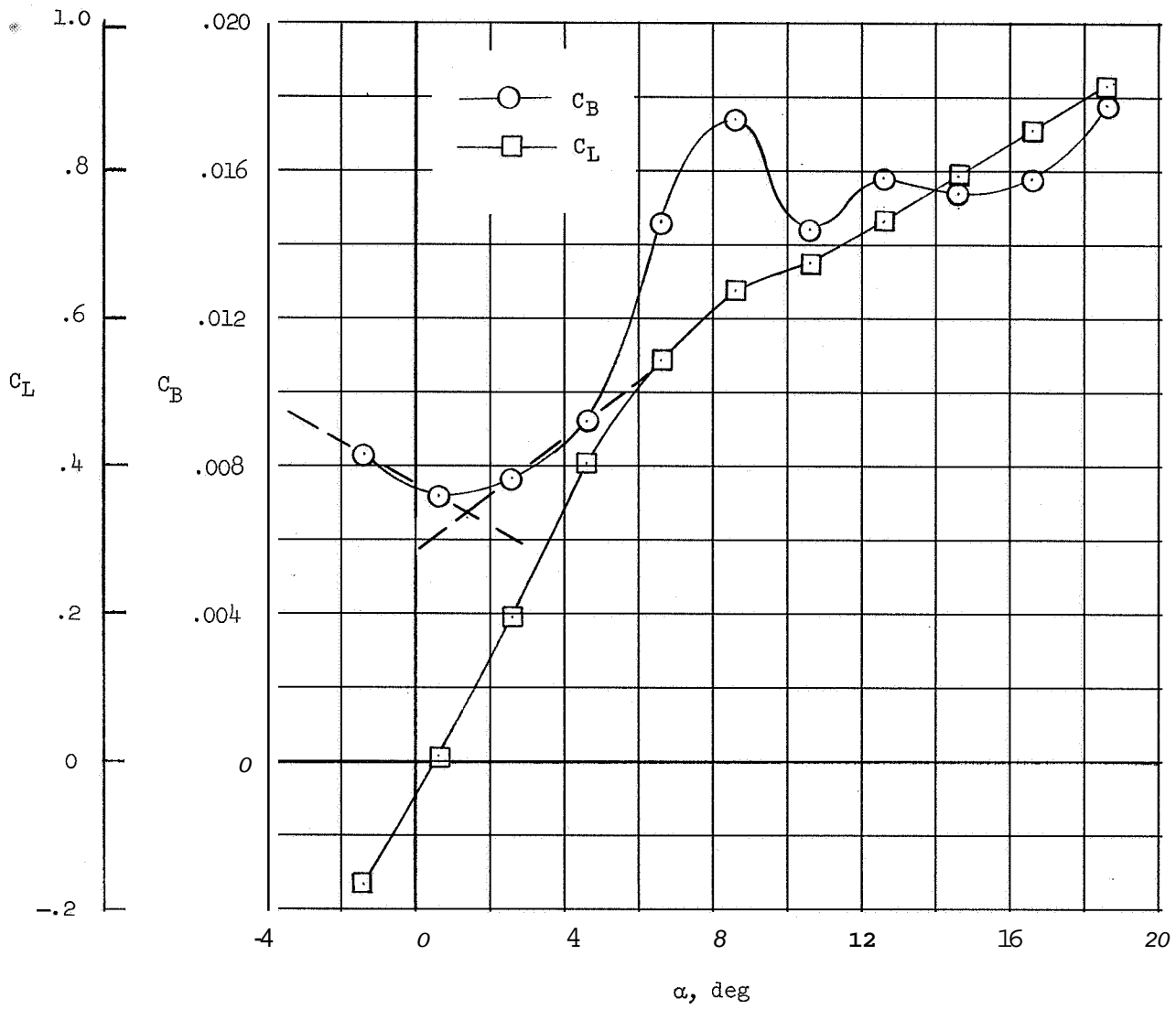
(d) M = 0.83.

Figure 8.- Continued.
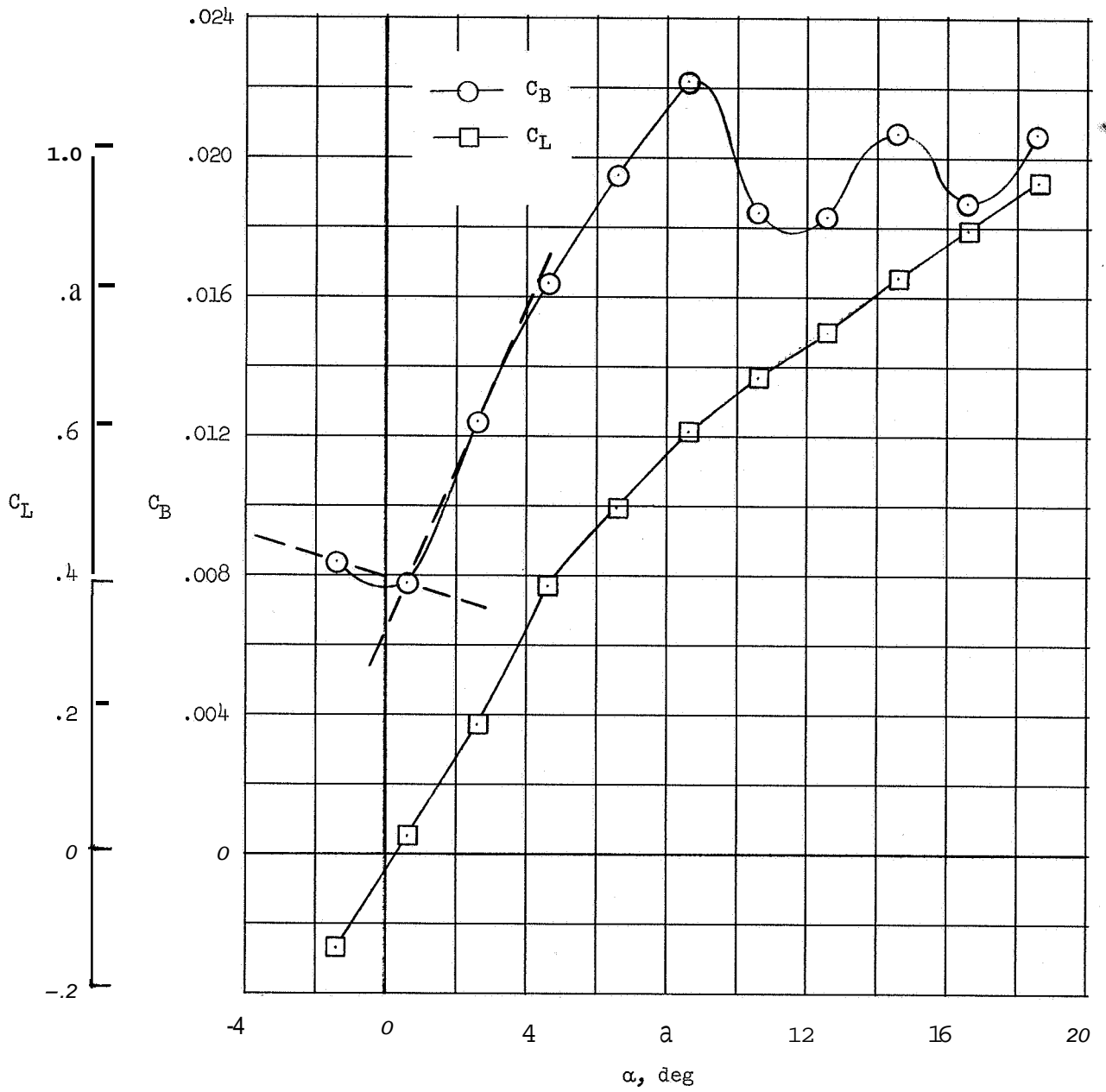
(e) M = 0.875.

Figure 8.- Continued.
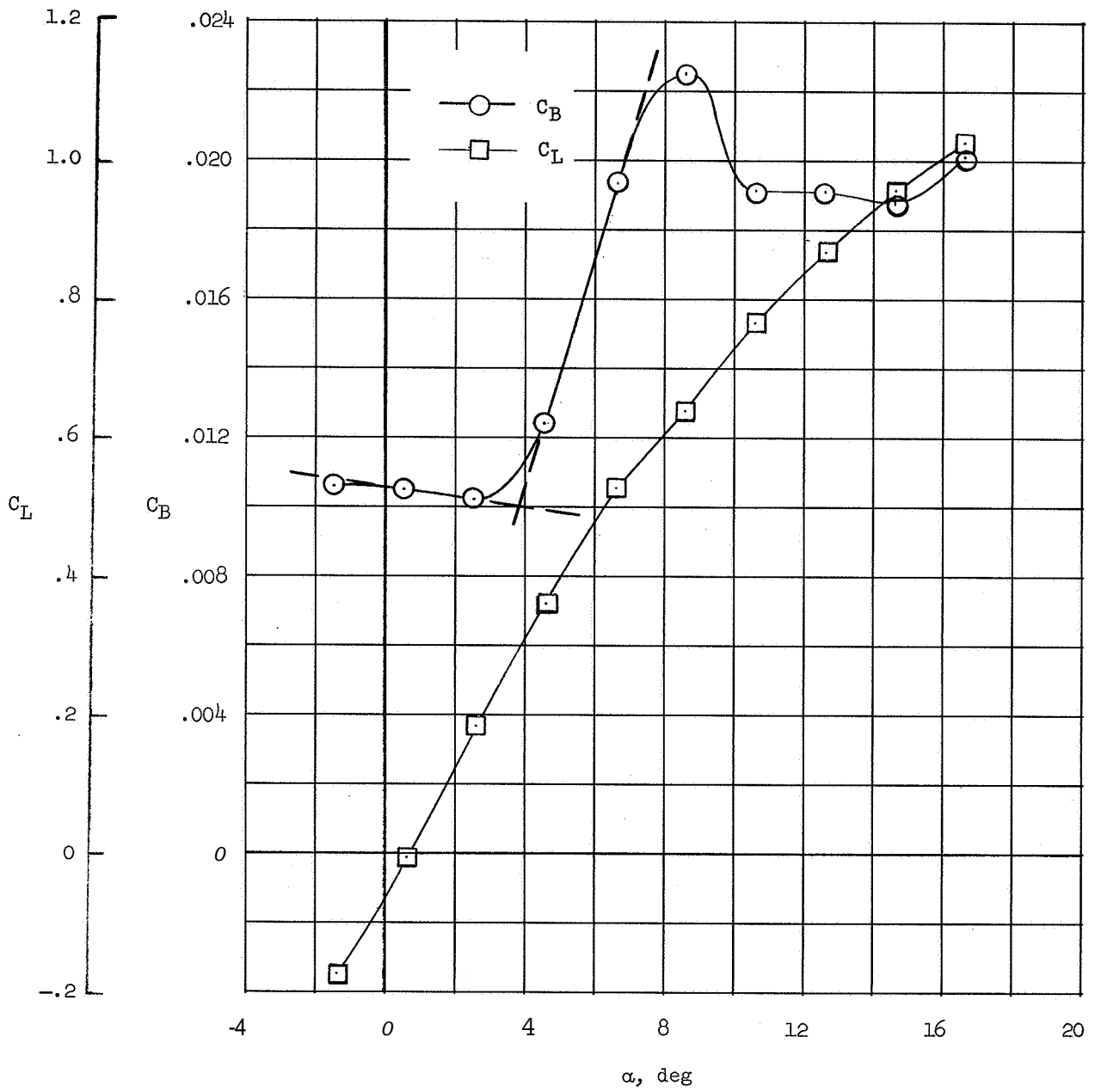
(f) M = 0.92.

Figure 8.- Concluded.
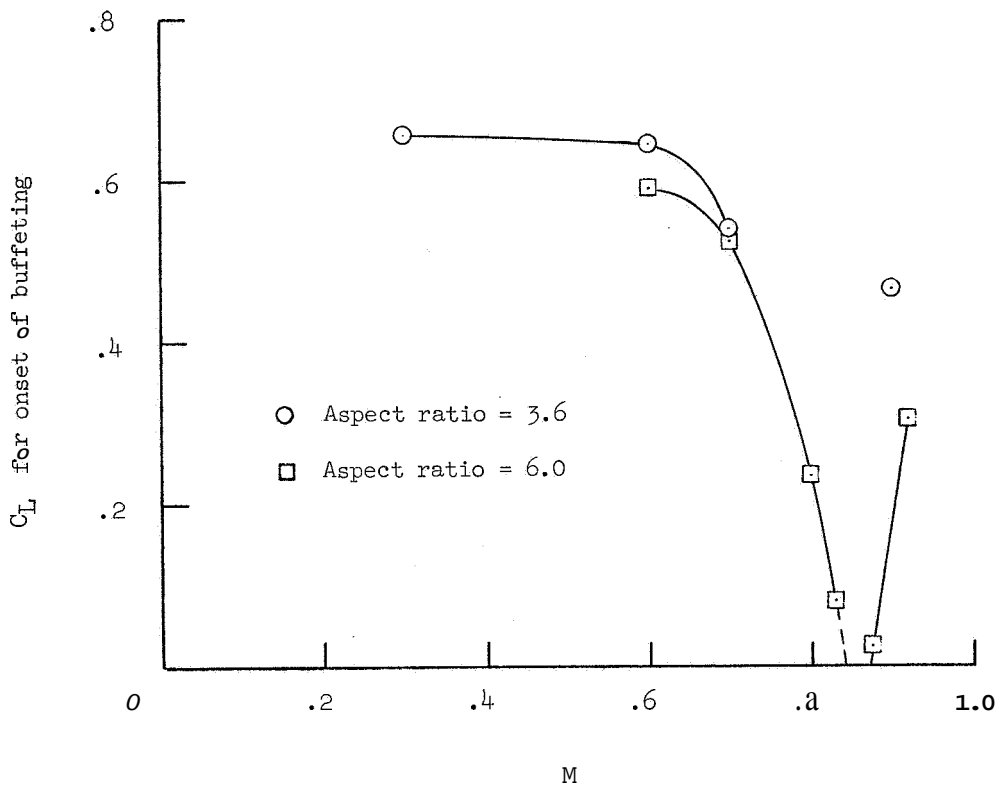
Figure *9.-* Comparison of buffet boundaries for the low-aspect-ratio *(3.6)* and high-aspect-ratio **(6.0)** wing configurations.

NASA SCIENTIFIC AND TECHNICAL PUBLICATIONS

TECHNICAL REPORTS: Scientific and technical information considered important, complete, and a lasting contribution to existing knowledge.

TECHNICAL NOTES: Information less broad in scope but nevertheless of importance as a contribution to existing knowledge.

TECHNICAL MEMORANDUMS: Information receiving limited distribution because of preliminary data, security classification, or other reasons.

CONTRACTOR REPORTS: Scientific and technical information generated under a NASA contract or grant and considered an important contribution to existing knowledge.

TECHNICAL TRANSLATIONS: Information published in a foreign language considered to merit NASA distribution in English.

SPECIAL PUBLICATIONS: Information derived from or of value to NASA activities. Publications include conference proceedings, monographs, data compilations, handbooks, sourcebooks, and special bibliographies.

TECHNOLOGY UTILIZATION PUBLICATIONS: Information on technology used by NASA that may be of particular interest in commercial and other non-aerospace applications. Publications include Tech Briefs, Technology Utilization Reports and Notes, and Technology Surveys.

Details on the availability of these publications may be obtained from:

SCIENTIFIC AND TECHNICAL INFORMATION DIVISION

NATIONAL AERONAUTICS AND SPACE ADMINISTRATION

Washington, D.C. 20546